Transport pathways and signatures of mixing in the extratropical tropopause region derived from Lagrangian model simulations

B. Vogel,[1] L. L. Pan,[2] P. Konopka,[1] G. Günther,[1] R. Müller,[1] W. Hall,[2] T. Campos,[2] I. Pollack,[2,3] A. Weinheimer,[2] J. Wei,[4,5] E. L. Atlas,[6] and K. P. Bowman[7]

Received 6 August 2010; revised 30 October 2010; accepted 23 November 2010; published 15 March 2011.

[1] Model simulations with the Chemical Lagrangian Model of the Stratosphere (CLaMS) driven by wind fields of the National Center for Environmental Prediction (NCEP) were performed in the midlatitude tropopause region in April 2008 to study two research flights conducted during the START08 campaign. One flight targeted a deep tropospheric intrusion and another flight targeted a deep stratospheric intrusion event, both of them in the vicinity of the subtropical and polar jet. Air masses with strong signatures of mixing between stratospheric and tropospheric air masses were identified from measured CO-O_3 correlations, and the characteristics were reproduced by CLaMS model simulations. CLaMS simulations in turn complement the observations and provide a broader view of the mixed region in physical space. Using artificial tracers of air mass origin within CLaMS yields unique information about the transport pathways and their contribution to the composition in the mixed region from different transport origins. Three different regions are examined to categorize dominant transport processes: (1) on the cyclonic side of the polar jet within tropopause folds where air from the lowermost stratosphere and the cyclonic side of the jet is transported downward into the troposphere, (2) on the anticyclonic side of the polar jet around the 2 PVU surface air masses, where signatures of mixing between the troposphere and lowermost stratosphere were found with large contributions of air masses from low latitudes, and (3) in the lower stratosphere associated with a deep tropospheric intrusion originating in the tropical tropopause layer (TTL). Moreover, the time scale of transport from the TTL into the lowermost stratosphere is in the range of weeks whereas the stratospheric intrusions occur on a time scale of days.

Citation: Vogel, B., et al. (2011), Transport pathways and signatures of mixing in the extratropical tropopause region derived from Lagrangian model simulations, *J. Geophys. Res.*, *116*, D05306, doi:10.1029/2010JD014876.

1. Introduction

[2] Two-way stratosphere-troposphere exchange (STE) in the extratropical tropopause region plays an important role in trace gas composition in the upper troposphere and lower stratosphere (UTLS). Changes in the concentration of radiatively active species in this region will affect radiative forcing. Therefore, quantifying STE is an essential step toward understanding and predicting future climate change [e.g., *Manabe and Weatherald*, 1967; *Rind et al.*, 1996; *Forster and Shine*, 2002; *Randel et al.*, 2007; *Intergovernmental Panel on Climate Change*, 2007; *Solomon et al.*, 2010]. In order to diagnose and quantify transport and mixing in the UTLS, model tools are required permitting observed STE events to be reproduced. Here, the impact of transport on the chemical composition in the UTLS, in particular the signature of mixing processes and transport pathways, will be analyzed using tracers of air mass origin in Lagrangian simulations.

[3] In situ measurements of trace gases show that a layer around the extratropical tropopause can be characterized as a mixture of tropospheric and stratospheric air masses. This layer is referred to as the extratropical transition layer (ExTL) [e.g., *Danielsen*, 1968; *Shapiro*, 1980; *Kritz et al.*, 1991; *Hoor et al.*, 2004; *Pan et al.*, 2004; *Hoor et al.*, 2005; *Pan et al.*, 2007; *Hegglin et al.*, 2009]. Extratropical STE is associated with synoptic-scale and mesoscale pro-

[1]Institute of Energy and Climate Research - Stratosphere, Forschungszentrum Jülich, Jülich, Germany.
[2]Atmospheric Chemistry Division, National Center for Atmospheric Research, Boulder, Colorado, USA.
[3]Chemical Sciences Division, Earth System Research Laboratory, National Oceanic and Atmospheric Administration, Boulder, Colorado, USA.
[4]Center for Satellite Application and Research, NESDIS, NOAA, Camp Springs, Maryland, USA.
[5]NASA Goddard Space Flight Center, Code 610.2, Greenbelt, Maryland, USA.
[6]Division of Marine and Atmospheric Chemistry, Rosenstiel School of Marine and Atmospheric Science, University of Miami, Miami, Florida, USA.
[7]Department of Atmospheric Sciences, Texas A&M University, College Station, Texas, USA.

0148-0227/11/2010JD014876

cesses; therefore the ExTL does not have a uniform depth near the tropopause, but rather has strong spatial variations [*Pan et al.*, 2007].

[4] For example, tropopause folds, which are also referred to as stratospheric intrusions, occur episodically and lead to irreversible transport of stratospheric air into the troposphere in the vicinity of the jet streams [e.g., *Danielsen*, 1968; *Shapiro*, 1980; *Vaughan et al.*, 1994; *Baray et al.*, 2000; *Sprenger et al.*, 2003]. In tropopause folds an extensive layer of mixed stratospheric and tropospheric air is found on the cyclonic (poleward) side of the jet [*Pan et al.*, 2007]. Here, the thermal tropopause [*World Meteorological Organization*, 1957] is less well defined, and there is a substantial vertical separation between the thermal tropopause and the surface with a constant potential vorticity of two potential vorticity units (1 PVU = 10^{-6} Km^2 kg^{-1} s^{-1}) referred to as 2 PVU surface. Further, there is evidence that mixing processes in stratospheric intrusions are associated with the wind shear of the jet streams [*Cho et al.*, 1999; *Pavelin and Whiteway*, 2002; *Pan et al.*, 2006, 2007].

[5] The lowermost stratosphere (LMS), which is the part of the extratropical stratosphere where isentropes intersect the tropopause, is often considered to be bounded by the 380 K isentrope above and the extratropical tropopause below. In the LMS, measurements show that a significant influence of tropospheric air is evident far above the extratropical tropopause [e.g., *Kritz et al.*, 1991; *Dessler et al.*, 1995; *Hintsa et al.*, 1998; *Vaughan and Timmis*, 1998; *Ray et al.*, 1999; *Hoor et al.*, 2004, 2005; *Bönisch et al.*, 2009]. This suggests that a substantial fraction of air in the LMS is isentropically mixed from the tropical upper troposphere [*Rosenlof et al.*, 1997; *Shepherd*, 2007; *Bönisch et al.*, 2009]. Recently, deep tropospheric intrusions observed in ozone measurements by satellites and sondes have been shown to be associated with low static stability [e.g., *Murgatroyd*, 1965; *Reid et al.*, 2000; *Tuck et al.*, 2003] and the presence of a secondary tropopause [*Pan et al.*, 2009].

[6] Mixing in the tropopause region is a key mechanism in irreversible STE. The effect of mixing is frequently identified from in situ aircraft measurements using tracer-tracer correlations [e.g., *Danielsen*, 1968; *Kelly et al.*, 1989; *Fischer et al.*, 2000; *Zahn and Brenninkmeijer*, 2002; *Hoor et al.*, 2002; *Pan et al.*, 2004; *Krebsbach et al.*, 2006; *Pan et al.*, 2006; *Kunz et al.*, 2009]. It is difficult, however, to quantify tracer transport resulting from mixing by using these observations alone. Trajectory studies using three-dimensional winds from meteorological data sets are often used to investigate the transport origins or to quantify transport [e.g., *Chen*, 1994, 1995; *Stohl*, 1998; *Seo and Bowman*, 2001, 2002; *Wernli and Bourqui*, 2002; *Sprenger and Wernli*, 2003; *Stohl et al.*, 2003; *Berthet et al.*, 2007; *Pan et al.*, 2007; *Bowman et al.*, 2007, and references therein]. Because pure trajectory models represent only advective transport by the resolved flow, trajectories by themselves do not represent or quantify mixing processes. Quantitative studies of mixing require models that can compute estimates of mixing. Several previous studies have shown that the Chemical Lagrangian Model of the Stratosphere (CLaMS), which uses the shear and deformation of the large-scale winds to parameterize mixing [*McKenna et al.*, 2002a, 2002b; *Konopka et al.*, 2007], has the ability to characterize mixing near the tropopause, in particular in tropopause folds [e.g., *Pan et al.*, 2006].

[7] Here, we compare CLaMS simulations with observations obtained during the Stratosphere-Troposphere Analyses of Regional Transport (START08) campaign [*Pan et al.*, 2010]. The START08 experiment was conducted using the U.S. National Science Foundation (NSF) Gulfstream V (GV) research aircraft, operated by the National Center for Atmospheric Research (NCAR). The experiment is designed to characterize the transport pathways in the extratropical tropopause region. A total of 18 research flights were conducted based out of Rocky Mountain Metropolitan Airport, Broomfield, Colorado, between April and June 2008. The flights sampled latitudes from 25°N–65°N and altitudes from the surface to ~14.5 km (~390 K potential temperature). In addition to meteorological variables, a large suite of chemical species and microphysical parameters was measured on the GV.

[8] The goal of this paper is to integrate the information from the aircraft observations and the CLaMS model to quantify and characterize signatures of mixing between stratospheric and tropospheric air. In this paper, the term "mixing" is used in the following senses: (1) mixing between stratospheric and tropospheric air masses which is evident in CO-O_3 tracer correlation and (2) mixing as result of the CLaMS mixing scheme that is parameterized by the deformation of the large-scale winds (see section 3.1). Our investigation focuses on two main questions. First, how well does CLaMS represent observed mixing in the tropopause region? Second, what can we learn from CLaMS simulations about transport and signatures of mixing observed during START08? The tropopause region is very challenging for global models, as most Eulerian Chemistry Climate Models (CCMs) are found to be too diffusive in this region [*Hegglin et al.*, 2010].

[9] The modeling and analysis in this paper focus on two START08 research flights (RF), RF01, conducted on 18 April to investigate a tropospheric intrusion event, and RF04, conducted on 28 April to investigate a stratospheric intrusion (tropopause fold event). To integrate CLaMS models and GV observations, we first compare signatures of mixing processes in CLaMS simulations with those observed using tracer-tracer correlations. This is followed by the analysis of artificial tracers of air mass origin in CLaMS simulations [*Günther et al.*, 2008]. The artificial tracer technique allows not only the origin of the air parcels to be identified but also the contribution of different air masses involved in observed mixed air.

2. Data

2.1. Meteorological Situation

[10] Research flight 1 (RF01), targeting a deep tropospheric intrusion, was conducted on 18 April 2008. The flight path was along a triangle from Broomfield, Colorado (39°N, 107°W), to North Ontario (56°N, 87°W) (part 1), continuing to near Milwaukee, Wisconsin (43°N, 88°W) (part 2), and then back to Broomfield (part 3) (see Figure 1a). A maximum altitude of ~14.5 km was reached. The air mass associated with the tropospheric intrusion is characterized by low values of both potential vorticity (PV) and static stability (buoyancy frequency squared, N^2) derived from NCEP data as shown in Figure 1. A double thermal tropopause (see Figure 1e, white dots) encloses the tropospheric intrusion centered around 380 K potential temperature with a vertical extension

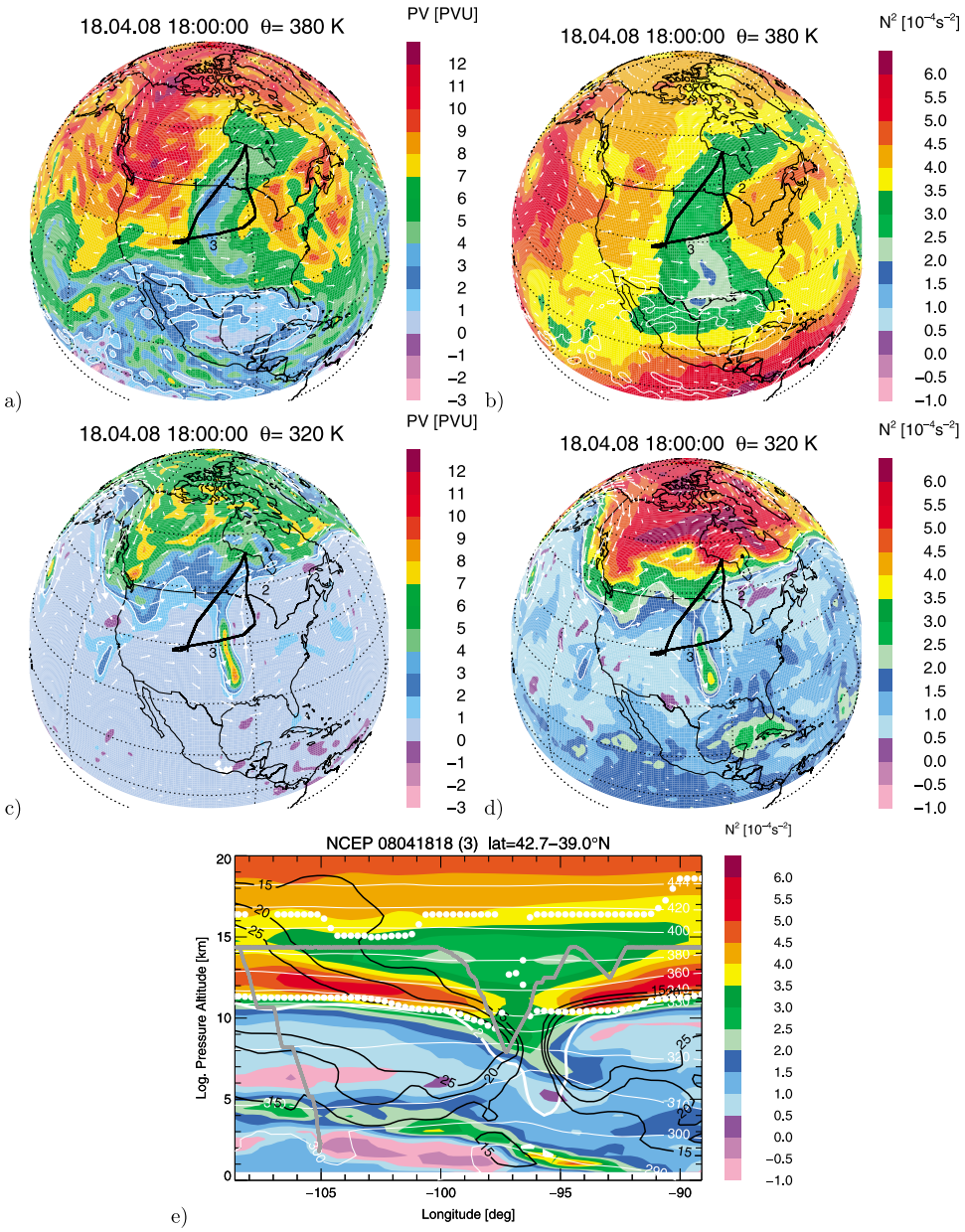

Figure 1. The horizontal distribution of PV and static stability (N^2) at (a and b) 380 K and (c and d) 320 K potential temperature on 18 April 2008. The 2 PVU isopleths for potential vorticity from NCEP data are marked by white contour lines. The horizontal winds are indicated by white arrows. The flight path for RF01 on 18 April 2008 is marked by the black triangle. (e) Static stability (N^2) within the curtain along the flight path (part 3 of the flight) as a function of altitude. The corresponding levels of potential temperature are marked by thin white lines. Further, the thermal tropopause (white dots), the 2 PVU surface (white thick line), and the flight path (gray thick line) are also shown. The magnitude of horizontal winds in m/s (black contours) indicates the position of the polar jet.

of approximately ±20 K (see Figure 1e). Further, during part 3 of the flight, a small tropopause fold was probed which was characterized by discrepancies between the first thermal tropopause (Figure 1e, lower row of white dots) and the 2 PVU surface (white thick line) in the vicinity of the polar jet (black lines). The fold is characterized by a strong horizontal PV gradient on the 320 K surface between air masses inside and outside the tropopause fold marked by the 2 PVU isoline which is associated with the location of the polar jet (see Figure 1c). Moreover, air masses in the tropopause fold are also characterized by higher N^2 compared to the tropospheric background. Because RF01 probed both a deep tropospheric intrusion and a tropopause fold during part 3 of the flight (see flight path Figure 1e, gray line), in the following analysis we focus on part 3 of the flight.

[11] RF04, performed on 28 April 2008, was flown roughly along 40° latitude from Broomfield, Colorado (39°N, 107°W), to Indianapolis, Indiana (40°N, 86°W), and back

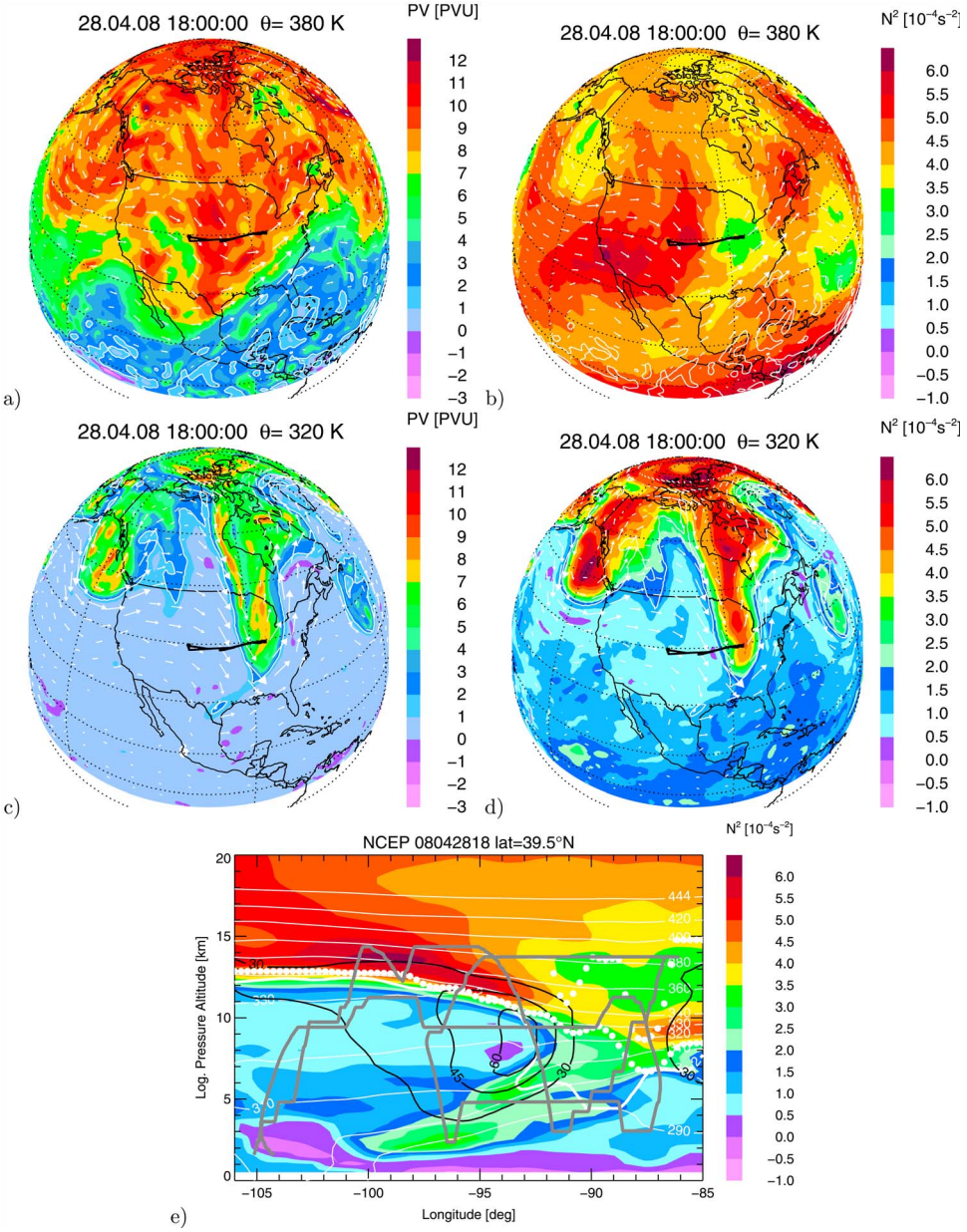

Figure 2. Same as Figure 1 but for research flight RF04 on 28 April 2008.

(see Figure 2a). The maximum altitude on this flight was also nearly 14.5 km. This flight sampled a deep tropopause fold over the central U.S. on the cyclonic flank of a northerly polar jet merged with the subtropical jet [*Pan et al.*, 2010]. Air masses within a deep stratospheric intrusion in the vicinity of the polar jet were sampled during the flight as shown in Figures 2c to 2e. Here also, the tropopause fold is characterized by a large difference between the thermal tropopause and the 2 PVU surface. A second thermal tropopause exists above the first one in the region above the tropopause fold. Relatively low values of N^2 compared to the stratospheric background are found between the two thermal tropopauses. In the stratospheric intrusion, N^2 values are relatively high compared to the tropospheric background (see Figures 2d and 2e).

2.2. Measured CO and O_3 Correlations

[12] Ozone (O_3) and carbon monoxide (CO) measurements on board GV are used in this study. The ozone data were obtained from a new NCAR instrument built for routine use on the GV. START08 is the instrument's first research deployment. The measurement principle of the instrument is based on chemiluminescence from the reaction of nitric oxide (NO) with ambient O_3 [*Ridley et al.*, 1992]. A 1 Hz sampling rate was used for the data presented here. The overall uncertainty of the O_3 is estimated to be ±3% of the ambient measured mixing ratio. The 1 s detection limit is 0.02 ppbv.

[13] The in situ CO measurements used in this study are from NCAR Research Aviation Facility (RAF) CO instrument. This instrument is a modified version of a commercial

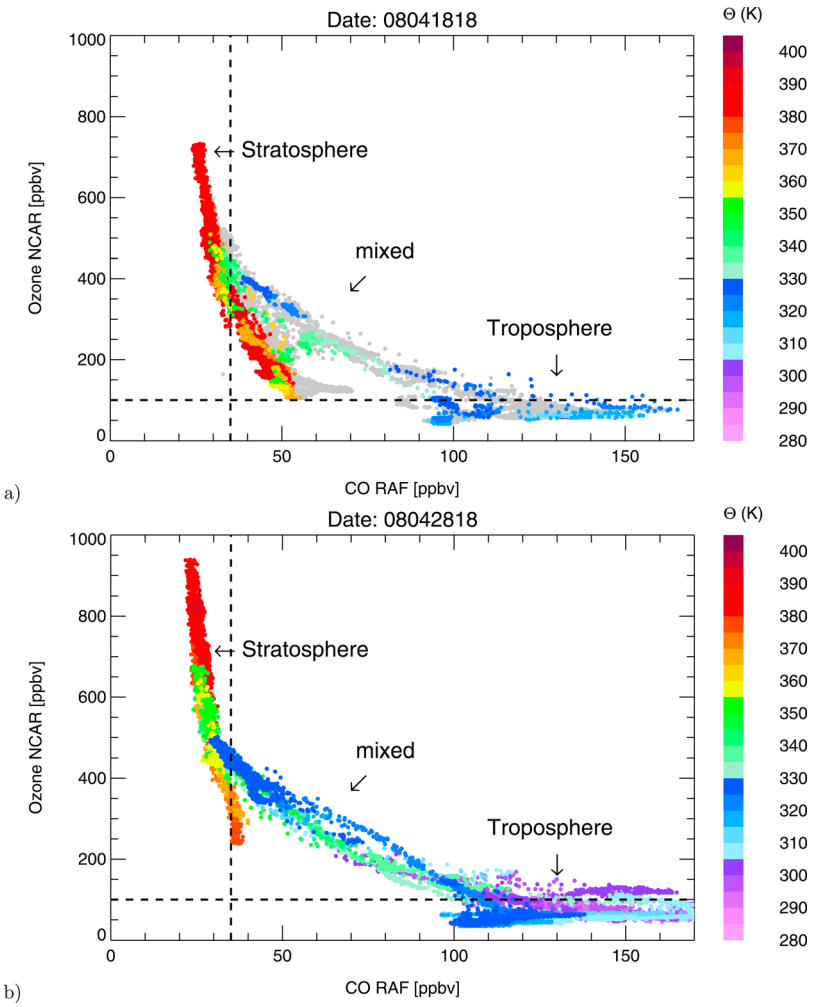

Figure 3. Observed CO-O_3 correlation color coded with the potential temperature (Θ) for research flight (a) RF01 on 18 April 2008 and (b) RF04 conducted on 28 April 2008. The mix-limit lines (dashed black lines) separate in tracer-tracer space the stratospheric (CO < 35 ppbv) and tropospheric (O_3 < 100 ppbv) reservoirs from the region where mixing between stratospheric and tropospheric air masses determines the composition of the air (CO > 35 ppbv and O_3 > 100 ppbv). For research flight RF01 (Figure 3a), only data from part 3 of the flight (see Figure 1) are color coded. Data from part 1 and 2 of the flight are shown in gray.

vacuum UV resonance fluorescence instrument [*Gerbig et al.*, 1999]. The CO instrument is operated at 1 Hz sampling rate and with an estimated uncertainty of ± (2 ppbv + 5%) for a 30 ppbv ambient mixing ratio. Postmission comparisons show a larger uncertainty for mixing ratios below 20–25 ppbv.

[14] Figure 3 shows measured CO-O_3 correlations [e.g., *Fishman and Seiler*, 1983] from research flight RF01 (Figure 3a) and RF04 (Figure 3b) color coded by potential temperature. To focus on air masses with mixed stratospheric and tropospheric characteristics, we separate the air masses into three groups: (1) background stratosphere, (2) background troposphere, and (3) mixed. Empirical criteria are used to identify the three groups in tracer space. The stratospheric background is chosen as air with CO < 35 ppbv. The tropospheric background is identified by O_3 < 100 ppbv. Air with O_3 > 100 ppbv and CO > 35 ppbv is considered to be mixed (see Figure 3). In Figure 3, these criteria are shown as "mix-limit lines" (dashed black lines) in the CO-O_3 tracer space. The air parcels between the two mixing-limit lines have a fairly compact tracer-tracer relationship. For both flights, the distributions in tracer space intersect the 35 ppbv CO limit near 450 ppbv of O_3, and intersect the 100 ppbv O_3 limit between 100 and 150 ppbv of CO.

[15] For RF01, only the data from part 3 of the flight are color coded. Points within the CO-O_3 correlation with potential temperatures larger than 360 K (red), low ozone, and low CO values (O_3 < 200 ppbv and 30 ppbv < CO < 60 ppbv) are noteworthy (see Figure 3a). These data are measured within the tropospheric intrusion, as indicated by low PV and low N^2 above the first thermal tropopause (see section 2.1).

[16] Further, it is evident that for both flights the mixed region consists of two or more separate mixing lines or segments which have similar slopes. The shift away from each other indicates that they connect different parts of the

tropospheric and stratospheric branch. These different segments are characterized by different levels of potential temperature. Air masses between ~330 and 350 K (green) are mostly found at the bottom side of the mixing region and air masses between ~300 and 330 K (blue) are mostly found at the top edge of the mixing region in CO-O_3 tracer space.

[17] The separation into distinct lines with different colors is probably largely due to the flight path of the aircraft during flight RF01 and RF04. Therefore, the distinct lines represent very individual air masses probed during the flight. Most likely the lines would overlap if additional nearby flight paths were available. However, triggered by the large separation into distinct lines, the question is raised whether spatially separated air masses in the CO-O_3 correlation space have different characteristics concerning the origin of the air masses and their spatial location in physical space.

3. The Model Study

3.1. Description of the CLaMS Model

[18] For the START08 campaign, model simulations with the Chemical Lagrangian Model of the Stratosphere (CLaMS) are performed. CLaMS was originally developed for the stratosphere [*McKenna et al.*, 2002a, 2002b; *Konopka et al.*, 2004] and was recently extended to the troposphere [*Konopka et al.*, 2007, 2010]. Here, we present CLaMS simulations for the Northern hemisphere that cover an altitude range from the surface up to the 500 K potential temperature (~20 km altitude) with a horizontal resolution of 50 km. The model has 35 vertical levels with a maximum vertical resolution of 200 m at the tropopause. The isentropic advection is driven by meteorological analysis winds from the National Centers for Environmental Prediction (NCEP).

[19] Above 100 hPa, the cross-isentropic velocities are derived from radiation calculations [*Morcrette*, 1991; *Zhong and Haigh*, 1995]. Below 100 hPa, the model smoothly transforms from the isentropic to the hybrid-pressure coordinate [*Konopka et al.*, 2007]. In this way, the effect of large-scale convective transport as represented in the vertical winds (ω) of the meteorological analysis (NCEP) is taken into account. In CLaMS, an initial distribution of the air parcels is transported according to trajectories with subsequent mixing. The mixing procedure inserts or removes air parcels into the irregular grid, where the distances between next neighbors are larger or lower than a critical value (for details see *Konopka et al.* [2004]). Here, we use a critical Lyaponov exponent $\lambda_c = 2.0$ as a mixing parameter applied after each advection step of 6 h. In this way, the mixing processes in CLaMS are parameterized as driven by vertical shear and horizontal strain in the large-scale winds, which have their largest values in the vicinity of the jet streams.

[20] In this work, we are interested in studying the pathways of transport and the origins of air masses for air parcels observed during RF01 and RF04. For these air parcels observed CO-O_3 correlations are available. Therefore, the CLaMS simulations are performed with simplified chemistry, including methane oxidation, which is the most important chemical source of CO in the stratosphere. Also, loss of CO by reaction with OH is included in the simulations.

[21] The simulation is initialized on 1 April 2008, with CO and O_3 from a 3-D multiannual, global CLaMS simulation [*Konopka et al.*, 2010] performed from surface up to the stratopause, and follows the model setup described [*Konopka et al.*, 2007]. This multiannual simulation is available over the time period from October 2001 up to the present with 100 km horizontal resolution and the highest resolution of 400 m around 380 K potential temperature.

[22] CO values retrieved by the Atmospheric Infrared Sounder (AIRS) on the NASA Aqua satellite are used to prescribe CO sources at the Earth's surface [*Susskind et al.*, 2003]. Daytime global gridded data from the AIRS version 5 CO support product (100 vertical layers) are used to infer lower boundary conditions for noon each day. The AIRS data are interpolated on the lowest model level depending on latitude and longitude (3° × 3°) and are updated every 24 h during the CLaMS simulation.

[23] At the lower boundary ozone is set equal to zero, which means that no tropospheric source of O_3 is included in the simulation. At the upper boundary, O_3 is taken from the HALOE climatology [*Grooß and Russell*, 2005], while CO comes from the multiannual, global CLaMS simulation [*Konopka et al.*, 2010]. In the following, we use passively transported ozone in CLaMS to compare CLaMS with measurements. That means O_3 chemistry is neglected over the short period of the simulations.

[24] A tracer for estimating the mean age of air tracer in the current simulations is initialized from a climatological simulation with CLaMS [*Konopka et al.*, 2010]. Within the climatological simulation, the mean age of air is calculated from the time lag relative to a linearly increasing source within the boundary layer [*Waugh and Hall*, 2002]. The mean age at $\theta = 2500$ K is derived from Michelson Interferometer for Passive Atmospheric Sounding (MIPAS) observations of SF_6 [*Stiller et al.*, 2008]. A perpetual simulation of the first year (10 times from 1 October 2001 to 30 September 2002) defines a steady state of the model that is used as the initial state for the climatological simulation.

3.2. Tracers of Air Mass Origin in CLaMS

[25] To analyze the transport pathways during the two START08 flights, it is important to know where air masses originate in the CLaMS model. The CLaMS transport scheme consists of advection, which is the reversible part of transport (the trajectory), and mixing, the irreversible part of transport. Because of the mixing procedure in CLaMS, identification of the origin of an individual air parcel is not possible, unlike the case in a pure trajectory calculation, where air parcels are subject only to advection. However, this problem can be avoided by the use of artificial tracers of air mass origin that mark particular regions in the atmosphere (e.g., tropospheric or stratospheric air masses) [*Günther et al.*, 2008]. The idea of using artificial tracers to identify transport has been used for a long time in both Eulerian [e.g., *Mahlman and Moxim*, 1978; *Stone et al.*, 1999] and Lagrangian models [e.g., *Bowman and Cohen*, 1997; *Bowman and Carrie*, 2002]. This technique allows the relative contribution of air masses of varying origin to be quantified for every individual CLaMS air parcel. With this technique it is possible to quantify the origin of air masses and the pathways of transport leading to the simulated CO-O_3 correlation, with a focus on mixed air masses. In particular, transport pathways can be analyzed to help understand the observed tracer-tracer relationships.

Table 1. Definition of Artificial Tracers of Air Mass Origin Used to Initialize the CLaMS Model Simulations for 1 April 2008[a]

Tracer of Air Mass Origin	Latitude	PV	Θ
Low-latitude troposphere (LT)	0°–30°	<2 PVU	<355 K
Midlatitude troposphere (MT)	30°–60°	<2 PVU	<355 K
Polar troposphere (PT)	60°–90°	<2 PVU	<355 K
Tropical tropopause layer (TTL)	–	<2 PVU	355–425 K
Midlatitude lowermost stratosphere (MLS)	<60°	>2 PVU	<380 K
Polar lowermost stratosphere (PLS)	30°–60°	>2 PVU	<380 K
Lower stratosphere (LS)	–	>2 PVU	>380 K

[a]See also Figure 4.

[26] At beginning of the model run each particle is marked with a specific artificial tracer. That means, for example, that the stratospheric tracer (ST) for air parcels in the stratosphere is set equal to one and everywhere else equal to zero. Mixing in ClaMS between a stratospheric (ST = 1) and a tropospheric (ST = 0) air parcel is implemented by insertion of a new particle. The stratospheric tracer of the new particle is then equal to 0.5. Successive mixing processes between stratospheric and tropospheric air during the course of the simulation yield a tracer distribution differing from the initial distribution (ST = 1 or ST = 0).

[27] To study and quantify the pathways in CLaMS, a set of inert artificial tracers is introduced in the model. At the beginning of the simulation on 1 April 2008 the following tracers are defined (see Table 1 and Figure 4): tracers for low-latitude, midlatitude, and polar troposphere (LT, MT, and PT), tracers for the midlatitude and polar lowermost stratosphere (MLS and PLS), and tracers for the tropical tropopause layer (TTL) and lower stratosphere (LS).

[28] Figure 4 shows an idealized dynamical configuration for the initialization of the tracers of air mass origin. In this schematic, the polar jet (PJ in Figure 4) is plotted at high latitudes and the subtropical jet (STJ in Figure 4) at low latitudes. During both RF01 and RF04, however, the polar jet over North America was located in midlatitudes while the subtropical jet shifted poleward so that the two jets merged (see Figures 1 and 2).

4. Results

4.1. CLaMS Model Representation of CO-O_3 Relationship

[29] To examine how well the CLaMS mixing scheme reproduces observations, we compare the CO-O_3 relationship from CLaMS with data from START08. Since the GV observations represent roughly 200 m in each 1 s sample, while the model parcels represent roughly 50 km in the horizontal dimension, the comparisons involve significant sampling differences. Instead of interpolating the model output to the aircraft track, we chose to compare air from the entire model cross section that contains the aircraft flight track with that sampled by the aircraft. The comparisons therefore also serve to extend the observations to a greater physical space. Therefore, the model results are analyzed in a vertical plane (same as in Figures 1e and 2e) between the start and end point of the measurement up to the 500 K potential temperature surface (~20 km altitude). This is referred to as physical space. Indeed, in the modeled CO-O_3 relationship, air masses are included from regions that are not sampled by the observations. Therefore this is a pure qualitative comparison between observations and model. A more quantitative intercomparison follows in section 4.2.

[30] The model results are color coded according to the potential temperatures of the air parcels (Figure 5). Qualitatively, the modeled CO-O_3 relationship shows similar tracer space distributions to the observations (as shown in Figure 3) for the stratospheric branch and the mixed region. It is apparent, however, that the model underpredicts tropospheric CO values and the tropospheric branch in the modeled tracer space is not clearly defined. This is not surprising since the positive correlation between CO and O_3

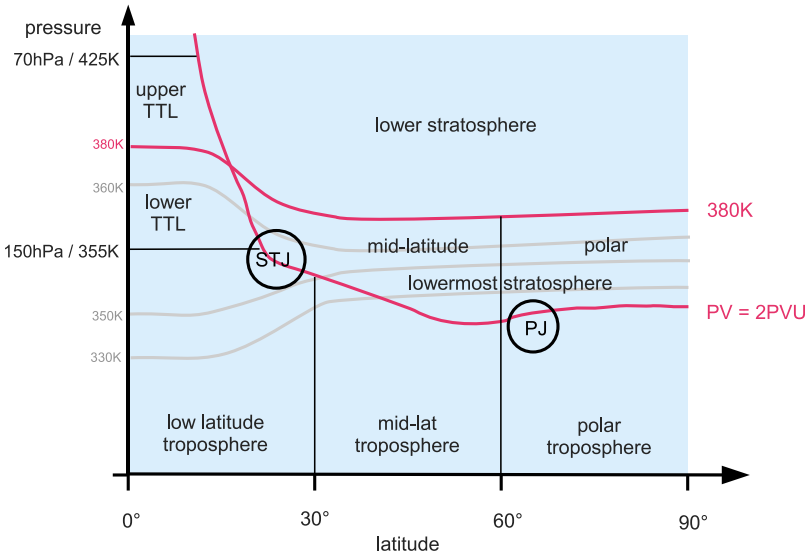

Figure 4. Defined regions marked with artificial tracers of air mass origin at the beginning of the simulation on 1 April 2008 (see also Table 1).

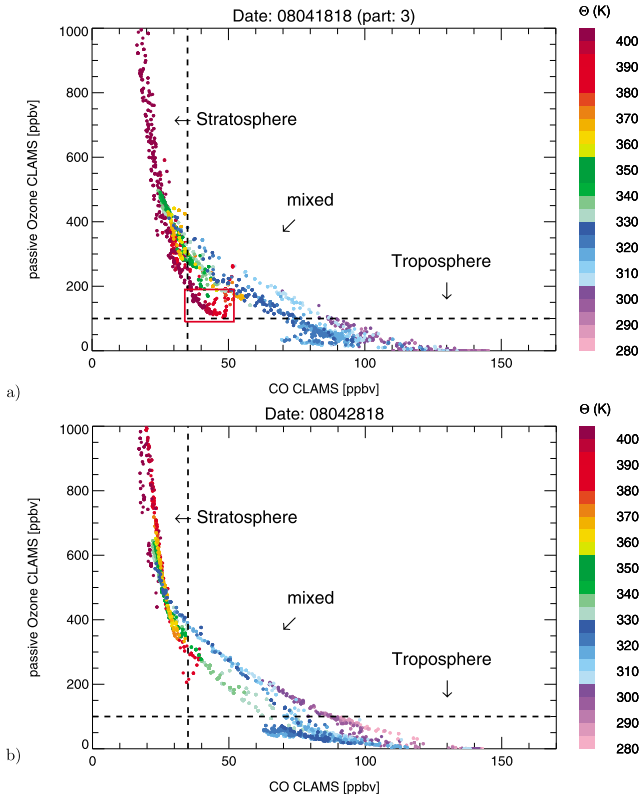

Figure 5. Simulated CO-O_3 correlation for all points along the vertical curtain of research flight (a) RF01 (part 3) and (b) RF04 color coded with the potential temperature. The air masses are separated into three groups: (1) background stratosphere (CO < 35 ppbv), (2) background troposphere (O_3 < 100 ppbv), and (3) mixed (O_3 > 100 ppbv and CO > 35 ppbv) marked by mix-limit lines (dashed lines). The box marks air masses with high potential temperature and both low CO and low O_3 values (see section 4.1).

seen in the observations (Figure 3) is often a result of both pollution transport (possibly convective) and chemistry (where CO is an O_3 precursor). Neither of these processes are represented due to the simplified chemistry scheme in CLaMS model. The insufficient tropospheric CO is also a main factor for several quantitative differences between the model and the observation. For example, the modeled mixing lines have different slopes compared to the observations. For the two flights the simulated mixing lines in tracer space intersect the CO mix-limit line (CO = 35 ppbv) between approximately 300 and 400 ppbv of O_3. At the tropospheric end they intersect the O_3 mix-limit line (O_3 = 100 ppbv) between approximately 70 ppbv and 90 ppbv of CO. The simulated values intersect the background limit lines in CO-O_3 coordinates at much lower CO and O_3 levels than in the observations.

[31] For RF01, CLaMS reproduces the observed behavior of the air parcels with high potential temperatures (greater than 370 K), low ozone and low CO (O_3 < 200 ppbv and 30 ppbv < CO < 60 ppbv; red dots within the red box in Figure 5a). In the case of research flight RF04, the CLaMS result is similar to the observations showing multiple segments that span the potential temperature range ~300–350 K.

[32] Further, the observations show (see Figure 3) that in tracer-tracer space the mixing region does not appear as a single mixing line, but rather as two or more separate mixing lines, which have a similar slope, but are shifted relative to each other indicating that they connect different parts of the tropospheric and stratospheric branch. This fact is also found in the CLaMS simulations. Within CLaMS, however, this separation is more pronounced than in the observations. In particular, this is evident for RF04 where air parcels between 300 and 330 K (blue-purple) are clearly separated from air parcels between 330 and 350 K (green). Reasons for this behavior will be discussed in section 5.

4.2. Signatures of Mixing Between Troposphere and Stratosphere

[33] The tracer space comparison in section 4.1 shows that CLaMS represents the mixed region well. Now we compare the modeled mixed region in physical space with the observation. Similar to the observations (see section 2.2), we separate the air masses from model simulations into three groups: (1) background stratosphere (CO < 35 ppbv), (2) background troposphere (O_3 < 100 ppbv), and (3) mixed (O_3 > 100 ppbv and CO > 35 ppbv). Projecting this information into the physical space, it is possible to compare in the model and the observation the location of air parcels exhibiting mixed chemical characteristics between the stratospheric and tropospheric reservoirs.

[34] Figures 6a and 6b show the simulated CO-O_3 correlations, and Figures 6c and 6d show the corresponding vertical cross sections indicating the mixed region in gray. Figures 6c and 6d allow us to compare the region of mixing inferred from CLaMS (gray) and the region of mixing along the flight path inferred from observations (yellow). The intercomparison between CLaMS and observations shows that for both research flights RF01 and RF04 the mixed regions agree qualitatively. However, overall the location of the mixed regions in CLaMS is slightly lower in altitude compared to the measurements. For example, on the anticyclonic side of the jet, a mixed region in CLaMS occurred just below the 2 PVU surface (in this region the thermal tropopause and the 2 PVU surface are very close to each other). On the other hand, the observations show a mixed region at or just above the 2 PVU surface. The reason for that is that the tropospheric branch in CLaMS is somewhat underrepresented compared to the observations as discussed in section 4.1. Despite the vertical offset in the altitude, the model results show physically realistic mixed regions for both flights and help expand the observations. The passive tracers in the model can further quantify the stratospheric and tropospheric contributions in the mixed region.

[35] The stratospheric tracer (ST), which is the sum of the midlatitude (MLS) and polar lowermost stratosphere (PLS) and of the lower stratosphere (LS), is very well suited for quantifying the relative contributions between the stratospheric and tropospheric reservoirs. Figures 6e and 6f show the stratospheric tracer (color coded) along the vertical cross section similar to Figures 6c and 6d. The mixed region defined by the CO and O_3 mix-limit lines is marked by white contour lines. An ST value larger than 99% means that the air parcel in CLaMS consists of pure stratospheric air, whereby air parcels with a lower fraction of ST tracer

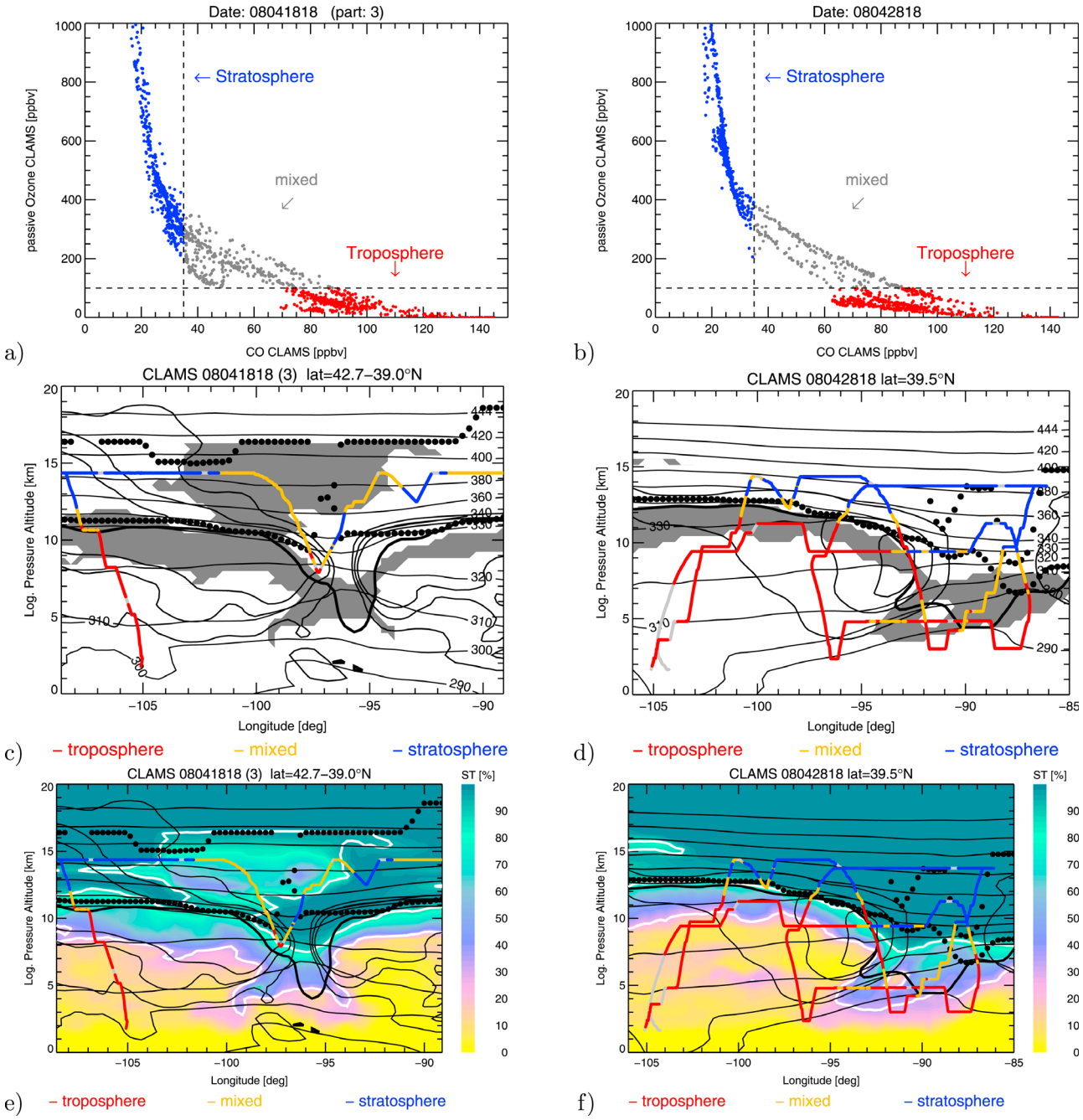

Figure 6. Simulated CO-O_3 correlation for all points along the curtain of (a) RF01 (part3) and (b) RF04. The stratospheric air masses are shown in blue (CO < 35 ppbv) and tropospheric air masses in red (O_3 < 100 ppbv). The region of air masses with signatures of mixing between stratospheric and tropospheric air is shown in gray (CO > 35 ppbv and O_3 > 100 ppbv). Location of mixed air masses in physical space for (c) RF01 and (d) RF04 from CLaMS (gray regions: CO > 35 ppbv and O_3 > 100 ppbv). Along the flight path regions of tropospheric (red, $O_{3measured}$ < 100 ppbv), mixed (yellow, $CO_{measured}$ > 35 ppbv and $O_{3measured}$ > 100 ppbv), and stratospheric (blue, $CO_{measured}$ < 35 ppbv) air masses are marked, deduced from observations. The corresponding levels of potential temperature are marked by thin black lines. Further, the thermal tropopause (black dots) and the 2 PVU surface (black thick line) are also shown. The magnitude of horizontal winds in m/s (black contours) indicates the position of the polar jet. The stratospheric tracer (ST) along the same cross section shown in Figures 6c and 6d for (e) RF01 and (f) RF04. The mix-limit lines for the stratosphere (CO = 35 ppbv) and for the troposphere (O_3 = 100 ppbv) used for the CLaMS simulations are indicated as white contour lines.

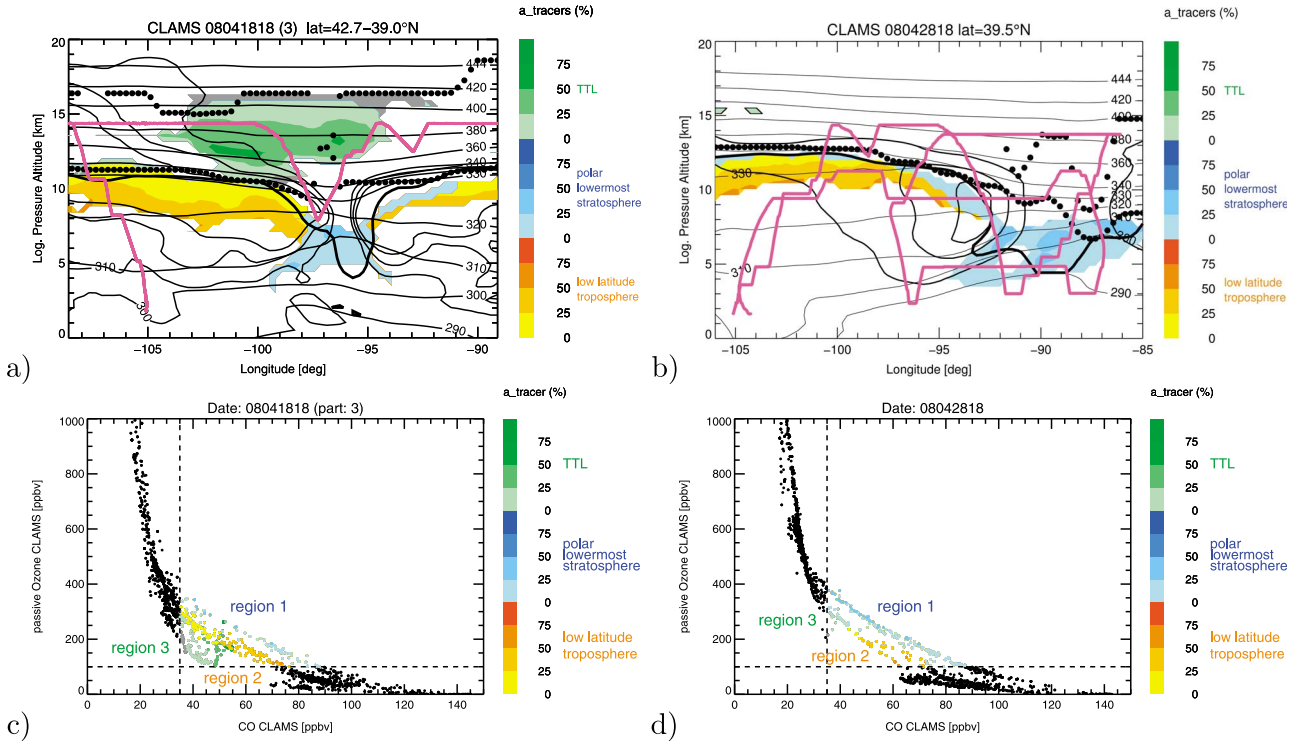

Figure 7. (a and b) Same cross section as in Figures 6c and 6d, but the location of mixed air masses in physical space (gray regions in Figures 6c and 6d) are color coded with different artificial tracers of air mass origin. Also, here, only regions with contributions of the low-latitude troposphere (yellowish/reddish), of the TTL (green) and of the polar lowermost stratosphere (blue) greater than 5% are shown to distinguish more easily between the different regions. (c and d) Same simulated CO-O_3 correlation as in Figures 6a and 6b, but the region with signatures of mixing between stratospheric and tropospheric air masses (CO > 35 ppbv and O_3 > 100 ppbv) is color coded with different artificial tracers of air mass origin. Only regions with contributions of the low-latitude troposphere (yellowish/reddish), of the TTL (green,) and of the polar lowermost stratosphere (blue) larger than 5% are shown to distinguish more easily between the different regions.

have contributions of the troposphere (sum of low-latitude (LT), midlatitude, and polar (PT) troposphere) or of the TTL.

[36] Figures 6e and 6f also show that air parcels just above the thermal tropopause do not consist of pure stratospheric air masses. This indicates that mixing between stratospheric and tropospheric air masses also occurred above the tropopause in the model in agreement with the observations. This shows that some signatures of mixing in physical space are sensitive to the criterion (mix-limit lines or ST tracer) used to characterize mixing signatures. However, in general, the signatures of mixing between stratospheric and tropospheric air masses show a good overall agreement between model results and observations.

4.3. Origin of the Air Masses and Transport Pathways

[37] The mixed region in the CO-O_3 correlations space for both observations and CLaMS results appears to have several lines or segments each characterized by a distinct range of potential temperature levels. This behavior suggests that the different segments in the tracer space may be formed by the mixing of air masses of different origins (see Figures 3 and 5). To analyze the origin of the air masses the artificial tracers introduced in section 3.2 are now discussed. These tracers make it possible to analyze and quantify the contributions from different global regions.

[38] Within the vertical curtain along the flight, we found three regions where tracers of air mass origin from several different, nonlocal regions [e.g., *Danielsen*, 1968] have significant contributions as shown in Figures 7a and 7b. In particular, region 1 (blue dots) has a significant contribution from the polar lowermost stratosphere and region 2 (yellowish/reddish dots) has a significant contribution from the low-latitude troposphere for both research flights RF01 and RF04. Region 3 (green dots) has a significant contribution from the TTL. Transforming the contributions of air mass origin to the simulated CO-O_3 correlations shows that the different regions identified in the physical space are clearly separated in the CO-O_3 correlation as three different segments (see Figures 7c and 7d). Thus, in tracer space, the CO-O_3 correlations are divided into three segments based on air mass origin from nonlocal regions. These segments correspond roughly to the following potential temperature levels: region 1 ~300–330 K, region 2 ~330–350 K and region 3 above 350 K). Thus, the regions 1 to 3 are separated both in the physical space and in the CO-O_3 correlation space. A small overlap of the different regions cannot be avoided.

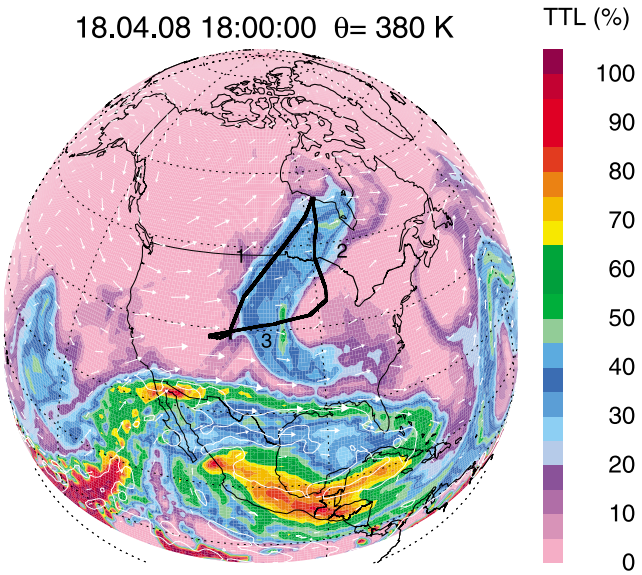

Figure 8. The horizontal distribution of the fraction of air masses originating in the tropical tropopause layer (TTL) at 380 K potential temperature on 18 April 2008. The 2 PVU isopleths for potential vorticity from NCEP data are marked by white contour lines. The horizontal winds are indicated by white arrows. The flight path for RF01 on 18 April 2008 is also marked (black triangle).

4.3.1. Research Flight RF01

[39] In research flight RF01, air masses within the tropospheric intrusion between the first and second tropopause have fractions of air masses originating from the TTL (green regions) with contributions of as much as 63%. Air masses within the tropopause fold have the highest contributions from the polar lowermost stratosphere of up to 37% (blue regions). Further, only air masses adjacent to the tropopause fold have large fractions of air masses from the low-latitude troposphere (yellowish/reddish regions). Here the 2 PVU surface constitutes a clear separation between air masses with fractions of tropospheric air masses from low latitudes, found below the 2 PVU surface, and stratospheric air masses above the 2 PVU surface. Analyzing the tropopause region of RF01 in more detail, we found that in the region where the contributions of the LT are larger than 20% air masses consist only of air parcels that contain significant fractions (>25%) of the LT, MT, and MLS. In general, air parcels in this region have contributions from the stratosphere and the troposphere in a similar range.

[40] Analyzing the tropospheric intrusion of RF01 in more detail, we found that in the region where the contributions of the TTL are larger than 20% the air masses contain only fractions of the TTL, MLS, and LS. It should be noted that there are no fractions of the PLS indicating that a transport barrier exists between the PLS and MLS. Most air parcels in this region have larger fractions (>50%) of stratospheric contributions compared to fractions of the TTL. This illustrates that mixing between air from the TTL and from the stratosphere occurred at the edge of the filament. In the core of the filament, there are still air masses with a high percentage of TTL air (up to 60%).

[41] Further, CLaMS simulation shows that 8–10 days before the tropospheric intrusion was observed during flight RF01, a filament of tropical air was separated from the TTL over Southeast Asia. During the first days of the simulation, air masses from the TTL (defined by PV < 2 PVU) are mixed with stratospheric air (PV > 2 PVU), thus the 2 PVU isopleth of the potential vorticity is not a strict transport barrier at altitudes around 380 K. The filament was then transported to midlatitudes over the Pacific Ocean to North America (see Figure 8). The fraction of air masses from the TTL within this filament has clearly decreased over time indicating that mixing with stratospheric air occurred. After 18 April 2008 the filament moves further eastward to the Atlantic Ocean and dissipates within approximately 10 days through mixing processes (see auxiliary material).[1]

[42] Moreover, the age of air in CLaMS is consistent with the results deduced from the analysis of the tracers of air mass origin as shown in Figure 9. Namely, air masses in the tropospheric intrusion are younger than the surrounding stratospheric air masses consistent with the notion that the air masses originate from the TTL. Further, air masses in the tropopause fold are older than air masses in the surrounding area indicating that the air masses have descended from the stratosphere into the polar lowermost stratosphere in the polar region.

4.3.2. Research Flight RF04

[43] Research flight RF04 observed a different dynamical situation than RF01, namely a deep stratospheric intrusion (see section 2). Nevertheless, the same types of air mass origin are found in research flights RF01 and RF04. Our simulations show that within the deep tropopause fold, up to 60% of the air masses originate from the polar lowermost stratosphere (see Figure 7b, blue region). Analyzing the stratospheric intrusion of RF04 in more detail, we found that in the region where the contributions of the PLS are larger than 20% air masses consists only of air parcels containing significant fractions (>25%) of the PLS, MLS, and MT. Most air parcels in this region have larger fractions (>50%) of stratospheric contributions compared to fractions of the troposphere indicating that air masses from the lowermost stratosphere were transported downward into the troposphere within the tropopause fold.

[44] Air masses on the anticyclonic side of the jet (westward of the tropopause fold) show a large contribution of tropospheric air from low latitudes (yellowish/reddish region).

[45] Model simulations show that air masses with small fractions from the TTL are found above the first tropopause between 380 and 400 K potential temperature (see Figure 7b, green region marked with black contours). Unfortunately, no observations are available in this region. These air masses are associated with low static stability (lower than in the surrounding stratospheric air; see Figure 2e) [e.g., *Murgatroyd*, 1965; *Reid et al.*, 2000; *Tuck et al.*, 2003] and low stratospheric tracer (see Figure 6f). These air masses are remnants of a filament originating in the TTL (see auxiliary material). This filament was separated from the TTL approximately 20 days before it was seen within the vertical cross section of flight RF04.

[1] Auxiliary materials are available in the HTML. doi:10.1029/2010JD014876.

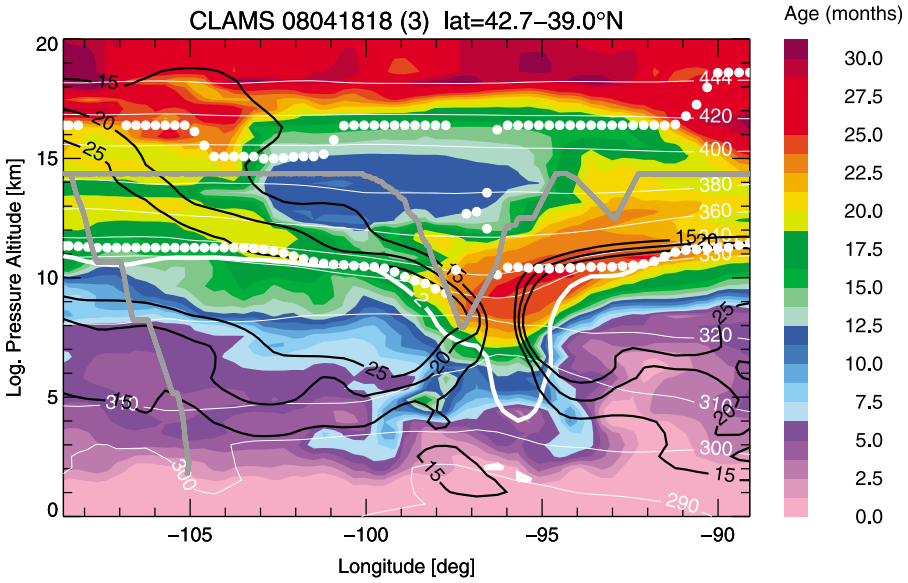

Figure 9. Mean age of air simulated with CLaMS for RF01 within the curtain along the flight path (part 3 of the flight) as a function of altitude. The remaining notation is the same as in Figure 1e.

[46] Similar to RF01, the age of air in CLaMS is consistent with the results deduced from tracers of air mass origin for research flight RF04 (not shown here). Air masses within the stratospheric intrusion are older (≈20 months) than the tropospheric air next to the fold, indicating that older stratospheric air masses were transported downward into the troposphere. Further, the small intrusion of air masses from the TTL above the thermal tropopause is also noticeable in the simulated mean age of air. Here, the air masses are younger (≈5 months) than the surrounding stratospheric air indicating that the air originates from the TTL.

5. Discussion

[47] In section 5.1, we will present the common principles found in CLaMS simulations for both research flights RF01 and RF04. In section 5.2, several open issues will be discussed.

5.1. Common Principles

[48] In general, in both flights, three different regions characterized by a different tracer of air mass origins are found: stratospheric intrusion (region 1), the tropopause region (region 2), and tropospheric intrusion (region 3). Each region is characterized by specific transport paths.

[49] 1. On the cyclonic side of the polar jet, air masses from the midlatitude and polar lowermost stratosphere are well mixed within the four weeks of simulation. Thus, after approximately 4 weeks of simulation, the lowermost stratosphere on the cyclonic side of the polar jet consists of roughly half polar and half midlatitude air from the lowermost stratosphere. Therefore, air in the stratospheric intrusions observed during RF01 and RF04, lying on the poleward side of the jet, has contributions from the polar lowermost stratosphere (see Figures 7c and 7d) and the midlatitude lowermost stratosphere.

[50] Results from both flights show that the air masses from the lowermost stratosphere were transported downward into the troposphere within the tropopause fold. This is consistent with previous studies [e.g., *Danielsen*, 1968; *Shapiro*, 1980; *Vaughan et al.*, 1994; *Baray et al.*, 2000; *Sprenger et al.*, 2003; *Pan et al.*, 2006, 2007]. The stratospheric intrusion yielded a deep extratropical transition layer, which is strongly influenced by mixing, in agreement with *Pan et al.* [2010]. In region 1 the stratospheric and tropospheric air are still separated. Integration of mixing events in CLaMS along 10 days backward trajectories shows that the stratospheric intrusions observed during RF01 and RF04 are not older than a few days associated with the lifetime of the tropopause fold.

[51] 2. The regions around the tropopause (outside the tropopause folds) on the equatorward side of the jet are characterized by air parcels with high fractions of the low-latitude troposphere (LT). This illustrates that in the model air masses from the low-latitude troposphere were transported into the midlatitude troposphere in agreement with previous studies [e.g., *Bowman and Carrie*, 2002].

[52] In general, air parcels in this region have contributions from the stratosphere and the troposphere in a similar range indicating that stratospheric and tropospheric air masses make a roughly equal contribution to mixing processes in the tropopause region. That means that air masses in region 2 are well mixed between stratospheric and tropospheric contributions. Mixed region 2 corresponds to the ExTL in the spatial extension observed during START08 and other observations [*Hoor et al.*, 2004; *Pan et al.*, 2004; *Hoor et al.*, 2005; *Pan et al.*, 2007].

[53] 3. CLaMS simulations illustrate that in tropospheric intrusions air from the TTL is transported into the lower and lowermost stratosphere and is still separated from stratospheric air. Our model results show that tropospheric intrusions into the lowermost stratospheric midlatitudes are not a singular event but rather a phenomenon that frequently

occurs in April over the Northern Hemisphere (see Figure 8 and auxiliary material). Further, our simulations show that the tropospheric intrusions observed during RF01 have a lifetime of approximately 20 days, in contrast to stratospheric intrusions.

[54] Our simulations support results from previous aircraft observations indicating that in the lowermost stratosphere a significant amount of tropospheric air is present [e.g., *Ray et al.*, 1999; *Hoor et al.*, 2004, 2005]. Our findings demonstrate that the origin of tropospheric intrusions is the tropical tropopause layer, as previously suggested [*Reid et al.*, 2000; *Bönisch et al.*, 2009].

5.2. Open Issues

[55] 1. Three tracers of air mass origin for the troposphere are introduced into CLaMS with boundaries at 30° and 60° latitude to divide the troposphere into different geographical regions. Our findings show that a very high percentage of air in region 2 originates in the low-latitude troposphere (LT), which is defined as less than 30°N and 2 PVU. The question is whether these air mass originate deep in the tropics or in the subtropics. To answer this question we analyzed further artificial tracers of air mass origin, which are also included in CLaMS in addition to the tracers described in section 3.2. Artificial tracers that mark latitudes <20°N and latitudes between 20°N and 30°N show that the main contributions of tropospheric air from low latitudes are from the subtropics (20°N–30°N) and not from the deep tropics. Nevertheless, for both flights air from equatorward of 20°N has a significant impact on region 2 in the range between 10% and 50%. In contrast, for RF01 the impact of air masses with latitudes <20°N is somewhat lower.

[56] 2. In CLaMS regions 1 and 2 are located at slightly lower altitudes than observed. Previous studies show that the extratropical tropopause layer (ExTL) extends about 25 K in potential temperature or 2–3 km altitude above the local tropopause (represented by 2 PVU surface) and is mainly influenced by the extratropical troposphere [*Hoor et al.*, 2004; *Pan et al.*, 2004; *Hoor et al.*, 2005; *Pan et al.*, 2007]. Thus, region 2 corresponds to the ExTL in spatial extent, but in the model it is approximately 20 K too low compared to observations from START08 and previous campaigns. The reasons for this are most likely uncertainties in the vertical velocities [*Plöger et al.*, 2010; *Konopka et al.*, 2010] and insufficient representation of the tropospheric CO source yielding stratospheric signatures that are too high in the lowermost stratosphere in CLaMS.

[57] In detail, the concept of the hybrid vertical velocity discussed by *Konopka et al.* [2007] is used in CLaMS. Here, above 100 hPa, the cross-isentropic velocities are derived from radiation calculations [*Morcrette*, 1991; *Zhong and Haigh*, 1995]. Below 100 hPa, the model smoothly transforms from the isentropic to the hybrid-pressure coordinate derived from NCEP [*Konopka et al.*, 2007]. In this approach, it is not guaranteed that the zonally and annually averaged total mass fluxes vanish at each Θ level [*Rosenlof*, 1995]. Thus, uncertainties in the vertical velocities remain [*Konopka et al.*, 2010]. Further, in the current version of CLaMS the diffusive flux from the troposphere into the stratosphere is underestimated because mixing is only driven by the deformation in flow and not by the static stability as expected from the definition of the gradient Richardson number.

[58] 3. CLaMS simulations show a stronger separation of segments describing regions 1 and 2 within CO-O_3 correlations than observed. The individual segments have a tropospheric end point between approximately 80 and 100 ppbv CO in the simulations and between approximately 100 and 120 ppbv CO in the observations. This shift between measurement and model result is caused by the simplified representation of CO in the simulation causing an underestimation of tropospheric CO compared to observations. Further, in CLaMS at the lower boundary, we do not use the terrain-following vertical coordinate (ζ = p, rather than $\zeta = \sigma$). This weakness of the model at the lower boundary could be a further reason for the underestimation of CO in the model. Additionally, uncertainties in the vertical velocities or in the mixing scheme could also contribute to the more pronounced separation of mixing regions 1 and 2 in CLaMS compared to the observations.

[59] 4. Finally, the question remaining open from our studies is: How representative are our findings in a climatological sense? In particular the question of how representative the separation of mixing region 1 and mixing region 2 is in CLaMS and in the observations for spring conditions. In our study, we analyzed two very special dynamical situations. In both cases, the jet streams are not westerly winds (flowing west to east) as for idealized conditions. On the contrary, the jet streams have a meandering shape. During research flights RF01 and RF04 the jets flowed in a north to south direction and vice versa. Further, the polar jet and the subtropical jet were combined into one stream. Therefore the dynamical situation of both flights was atypical.

6. Summary and Conclusions

[60] Simulations were performed with the Chemical Lagrangian Model of the Stratosphere (CLaMS) with a horizontal resolution of 50 km and 35 vertical levels driven by wind fields of the National Centers for Environmental Prediction (NCEP). The results of the simulations were compared with CO and O_3 measurements from research flights RF01 and RF04 of the START08 campaign. RF01 was conducted on 18 April 2008 investigating a deep tropospheric intrusion and RF04 on 28 April 2008 observing a deep stratospheric intrusion. The model simulations were performed to accomplish two related objectives. The first one was to evaluate whether the observed mixed regions were adequately reproduced by the model. The second one was to characterize, using the model simulation, the transport pathways targeted by the aircraft observations. Our findings show that CLaMS is able to reproduce the characteristics of the observations in regions of mixed stratospheric and tropospheric air masses. Using measurement-based tracer criteria, the model results show a physically realistic extratropical transition layer. Contributions of different source regions are quantified by using seven inert artificial tracers. The transport pathways that contributed to mixing between stratospheric and tropospheric air masses are identified. Our model simulations show that the distinct mixing lines in CO-O_3 tracer correlations are results of mixing processes involving air

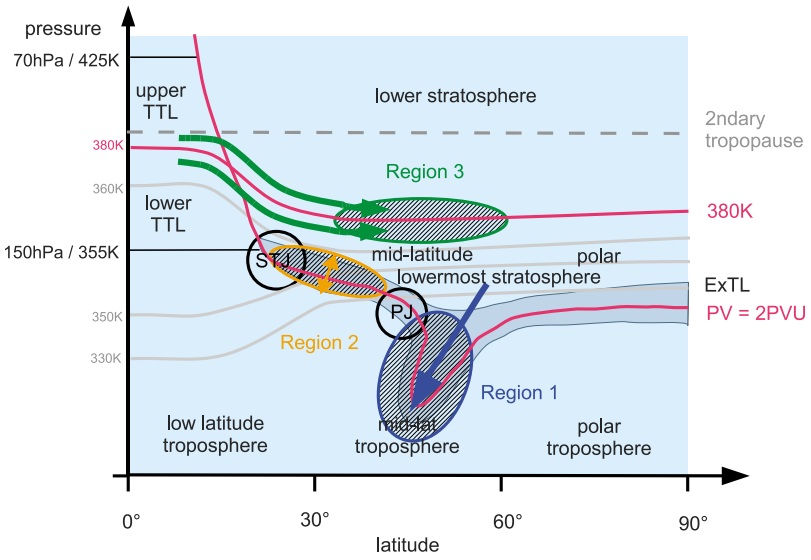

Figure 10. Locations of mixing (hatched areas) and transport pathways (arrows) found in CLaMS simulations (see section 6).

masses from different atmospheric regions nonlocal to the region of measurement.

[61] The CLaMS simulations show that for both research flight RF01 and RF04, which have different dynamical situations, the transport pathways and air mass origins in the mixed region can be characterized as shown in the schematic in Figure 10. Three components are identified based on their locations in tracer space and their isentropic ranges. Each has unique characteristics in its air mass origins, as follows.

[62] 1. Within stratospheric intrusions or tropopause folds, denoted as region 1 (see Figure 10, blue hatched area), air has significant contributions from the polar lowermost stratosphere, the midlatitude lowermost stratosphere, and the troposphere. Our simulations show that stratospheric air is transported downward into the troposphere within the tropopause fold. A mixing layer extends at an altitude of about 5–6 km altitude within the tropopause fold.

[63] 2. Air around the 2 PVU surface on the anticyclonic side of the polar jet corresponds to the ExTL (region 2; see Figure 10, orange hatched area). Our simulations show that air in this region is a mixture of stratospheric and tropospheric air masses and is strongly influenced by tropospheric air masses from low latitudes (<30°N) and from air masses from the midlatitude lowermost stratosphere.

[64] 3. Observations and model simulations show that deep tropospheric intrusions found above the first tropopause, denoted by mixed region 3 (see Figure 10, green hatched area), originate in the TTL (see Figure 10, green arrow). Filaments of TTL air separate from the TTL and move to higher latitudes in the stratosphere. Within these intrusions, mixing between air masses from the TTL and stratospheric air masses from the surrounding area occurs. Simulated tropospheric intrusions studied in this work have a lifetime of up to approximately 20 days before they can no longer be identified.

[65] Signatures of mixing processes between stratospheric and tropospheric air masses and the transport pathways in the ExTL and the lowermost stratosphere were identified for two research flights during START08. This extends our current knowledge about the extratropical UTLS region, in particular, it is confirmed by CLaMS simulations that tropospheric intrusions found in the lower stratosphere originate in the TTL.

[66] **Acknowledgments.** The authors thank three anonymous reviewers for their very helpful reviews. The START08 experiment is sponsored by the National Science Foundation (NSF). The authors gratefully acknowledge the instrument team, cosponsored by NFS and NCAR, and the NCAR Research Aviation Facility staff for running the flight operation. The work by B. Vogel was partly funded by the German Science Foundation (Deutsche Forschungsgemeinschaft, DFG) under contract 552102.

References

Baray, J.-L., V. Daniel, G. Ancellet, and B. Legras (2000), Planetary-scale tropopause folds in the southern subtropics, *Geophys. Res. Lett.*, *27*(3), 353–356.

Berthet, G., J. G. Esler, and P. H. Haynes (2007), A Lagrangian perspective of the tropopause and the ventilation of the lowermost stratosphere, *J. Geophys. Res.*, *112*, D18102, doi:10.1029/2006JD008295.

Bönisch, H., A. Engel, J. Curtius, T. Birner, and P. Hoor (2009), Quantifying transport into the lowermost stratosphere using simultaneous in-situ measurements of SF_6 and CO_2, *Atmos. Chem. Phys.*, *9*, 5905–5919.

Bowman, K. P., and G. D. Carrie (2002), The mean-meridional transport circulation of the troposphere in an idealized GCM, *J. Atmos. Sci.*, *59*(9), 1502–1514.

Bowman, K. P., and P. J. Cohen (1997), Interhemispheric exchange by seasonal modulation of the Hadley circulation, *J. Atmos. Sci.*, *54*(16), 2045–2059.

Bowman, K. P., L. L. Pan, T. Campos, and R. Gao (2007), Observations of fine-scale transport structure in the upper troposphere from the high-performance instrumented airborne platform for environmental research, *J. Geophys. Res.*, *112*, D18111, doi:10.1029/2007JD008685.

Chen, P. (1994), The permeability of the Antarctic vortex edge, *J. Geophys. Res.*, *99*(D10), 20,563–20,571.

Chen, P. (1995), Isentropic cross-tropopause mass exchange in the extratropics, *J. Geophys. Res.*, *100*(D8), 16,661–16,673.

Cho, J. Y. N., et al. (1999), Observations of convective and dynamical instabilities in tropopause folds and their contribution to stratosphere-troposphere exchange, *J. Geophys. Res.*, *104*(D17), 21,549–21,568.

Danielsen, E. F. (1968), Stratospheric-tropospheric exchange based on radioactivity, ozone and potential vorticity, *J. Atmos. Sci.*, *25*(3), 502–518.

Dessler, A. E., E. J. Hintsa, E. M. Weinstock, J. G. Anderson, and K. R. Chan (1995), Mechanisms controlling water vapor in the lower strato-

sphere: "A tale of two stratospheres," *J. Geophys. Res.*, *100*(D11), 23,167–23,172.

Fischer, H., F. G. Wienhold, P. Hoor, O. Bujok, C. Schiller, P. Siegmund, M. Ambaum, H. A. Scheeren, and J. Lelieveld (2000), Tracer correlations in the northern high latitude lowermost stratosphere: Influence of cross-tropopause mass exchange, *Geophys. Res. Lett.*, *27*(1), 97–100, doi:10.1029/1999GL010879.

Fishman, J., and W. Seiler (1983), Correlative nature of ozone and carbon monoxide in the troposphere: Implications for the tropospheric ozone budget, *J. Geophys. Res.*, *88*(C6), 3662–3670.

Forster, P., and K. P. Shine (2002), Assessing the climate impact of trends in stratospheric water vapor, *Geophys. Res. Lett.*, *29*(6), 1086, doi:10.1029/2001GL013909.

Gerbig, C., S. Schmitgen, D. Kley, A. Volz-Thomas, K. Dewey, and D. Haaks (1999), An improved fast-response vacuum-UV resonance fluorescence CO instrument, *J. Geophys. Res.*, *104*(D1), 1699–1704.

Grooß, J.-U., and J. M. Russell (2005), Technical note: A stratospheric climatology for O_3, H_2O, CH_4, NO_x, HCl, and HF derived from HALOE measurements, *Atmos. Chem. Phys.*, *5*, 2797–2807.

Günther, G., R. Müller, M. von Hobe, F. Stroh, P. Konopka, and C. M. Volk (2008), Quantification of transport across the boundary of the lower stratospheric vortex during Arctic winter 2002/2003, *Atmos. Chem. Phys.*, *8*, 3655–3670.

Hegglin, M. I., C. D. Boone, G. L. Manney, and K. A. Walker (2009), A global view of the extratropical tropopause transition layer from Atmospheric Chemistry Experiment Fourier Transform Spectrometer O_3, H_2O, and CO, *J. Geophys. Res.*, *114*, D00B11, doi:10.1029/2008JD009984.

Hegglin, M. I., et al. (2010), Multimodel assessment in the UTLS: Extratropics, *J. Geophys. Res.*, *115*, D00M09, doi:10.1029/2010JD013884.

Hintsa, E. J., et al. (1998), Troposphere-to-stratosphere transport in the lowermost stratosphere from measurements of H_2O, CO_2, N_2O and O_3, *Geophys. Res. Lett.*, *25*(14), 2655–2658, doi:10.1029/98GL01797.

Hoor, P., H. Fischer, L. Lange, J. Lelieveld, and D. Brunner (2002), Seasonal variations of a mixing layer in the lowermost stratosphere as identified by the CO-O_3 correlation from in situ measurements, *J. Geophys. Res.*, *107*(D5), 4044, doi:10.1029/2000JD000289.

Hoor, P., C. Gurk, D. Brunner, M. I. Hegglin, H. Wernli, and H. Fischer (2004), Seasonality and extent of extratropical TST derived from in-situ CO measurements during SPURT, *Atmos. Chem. Phys.*, *4*, 1427–1442.

Hoor, P., H. Fischer, and J. Lelieveld (2005), Tropical and extratropical tropospheric air in the lowermost stratosphere over Europe: A CO-based budget, *Geophys. Res. Lett.*, *32*, L07802, doi:10.1029/2004GL022018.

Intergovernmental Panel on Climate Change (2007), *Climate Change 2007: The Physical Science Basis. Contribution of Working Group I to the Fourth Assessment Report of the Intergovernmental Panel on Climate Change*, edited by S. Solomon et al., 996 pp., Cambridge Univ. Press, Cambridge, U. K.

Kelly, K. K., et al. (1989), Dehydration in the lower Antarctic stratosphere during late winter and early spring, 1987, *J. Geophys. Res.*, *94*(D9), 11,317–11,357.

Konopka, P., et al. (2004), Mixing and ozone loss in the 1999–2000 Arctic vortex: Simulations with the 3-dimensional Chemical Lagrangian Model of the Stratosphere (CLaMS), *J. Geophys. Res.*, *109*, D02315, doi:10.1029/2003JD003792.

Konopka, P., et al. (2007), Contribution of mixing to upward transport across the tropical tropopause layer (TTL), *Atmos. Chem. Phys.*, *7*, 3285–3308.

Konopka, P., J.-U. Grooß, G. Günther, F. Plöger, R. Pommrich, R. Müller, and N. Livesey (2010), Annual cycle of ozone at and above the tropical tropopause: Observations versus simulations with the chemical model of the stratosphere (CLaMS), *Atmos. Chem. Phys.*, *10*, 121–132.

Krebsbach, M., C. Schiller, D. Brunner, G. Günther, M. I. Hegglin, D. Mottaghy, M. Riese, N. Spelten, and H. Wernli (2006), Seasonal cycles and variability of O_3 and H_2O in the UT/LMS during SPURT, *Atmos. Chem. Phys.*, *6*, 109–125.

Kritz, M. A., S. W. Rosner, E. F. Danielsen, and H. B. Selkirk (1991), Air mass origins and troposphere-to-stratosphere exchange associated with mid-latitude cyclogenesis and tropopause folding inferred from ^{7}Be measurements, *J. Geophys. Res.*, *96*(D9), 17,405–17,414.

Kunz, A., P. Konopka, R. Müller, L. L. Pan, C. Schiller, and F. Rohrer (2009), High static stability in the mixing layer above the extratropical tropopause, *J. Geophys. Res.*, *114*, D16305, doi:10.1029/2009JD011840.

Mahlman, J., and W. Moxim (1978), Tracer simulation using a global general circulation model—Results from a midlatitude instantaneous source experiment, *J. Atmos. Sci.*, *35*, 1340–1374.

Manabe, S., and R. T. Weatherald (1967), Thermal equilibrium of the atmosphere with a given distribution of relative humidity, *J. Atmos. Sci.*, *24*, 241–259.

McKenna, D. S., J.-U. Grooß, G. Günther, P. Konopka, R. Müller, G. Carver, and Y. Sasano (2002a), A new Chemical Lagrangian Model of the Stratosphere (CLaMS): 2. Formulation of chemistry scheme and initialization, *J. Geophys. Res.*, *107*(D15), 4256, doi:10.1029/2000JD000113.

McKenna, D. S., P. Konopka, J.-U. Grooß, G. Günther, R. Müller, R. Spang, D. Offermann, and Y. Orsolini (2002b), A new Chemical Lagrangian Model of the Stratosphere (CLaMS): 1. Formulation of advection and mixing, *J. Geophys. Res.*, *107*(D16), 4309, doi:10.1029/2000JD000114.

Morcrette, J.-J. (1991), Radiation and cloud radiative properties in the European Centre for Medium-Range Weather Forecasts forecasting system, *J. Geophys. Res.*, *96*(D5), 9121–9132.

Murgatroyd, R. J. (1965), Ozone and water vapour in the upper troposphere and lower stratosphere, in *Meteorological Aspects of Atmospheric Radioactivity, WMO Ser.*, vol. 169, *169*, pp. 68–94, World Meteorol. Org., Geneva, Switzerland.

Pan, L. L., W. J. Randel, B. L. Gary, M. J. Mahoney, and E. J. Hintsa (2004), Definitions and sharpness of the extratropical tropopause: A trace gas perspective, *J. Geophys. Res.*, *109*, D23103, doi:10.1029/2004JD004982.

Pan, L. L., P. Konopka, and E. V. Browell (2006), Observations and model simulations of mixing near the extratropical tropopause, *J. Geophys. Res.*, *111*, D05106, doi:10.1029/2005JD006480.

Pan, L. L., et al. (2007), Chemical behavior of the tropopause observed during the Stratosphere-Troposphere Analyses of Regional Transport experiment, *J. Geophys. Res.*, *112*, D18110, doi:10.1029/2007JD008645.

Pan, L. L., W. J. Randel, J. C. Gille, W. D. Hall, B. Nardi, S. Massie, V. Yudin, and R. Khosravi (2009), Tropospheric intrusions associated with the secondary tropopause, *J. Geophys. Res.*, *114*, D10302, doi:10.1029/2008JD011374.

Pan, L. L., et al. (2010), The Stratosphere-Troposphere Analyses of Regional Transport 2008 (START08) experiment, *Bull. Am. Meteorol. Soc.*, *91*, 327–342.

Pavelin, E., and J. A. Whiteway (2002), Gravity wave interactions around the jet stream, *Geophys. Res. Lett.*, *29*(21), 2024, doi:10.1029/2002GL015783.

Plöger, F., P. Konopka, G. Günther, J.-U. Grooß, and R. Müller (2010), Impact of the vertical velocity scheme on modeling transport across the tropical tropopause layer, *J. Geophys. Res.*, *115*, D03301, doi:10.1029/2009JD012023.

Randel, W. J., M. Park, F. Wu, and N. Livesey (2007), A large annual cycle in ozone above the tropical tropopause linked to the Brewer-Dobson circulation, *J. Atmos. Sci.*, *64*, 4479–4488.

Ray, E., F. Moore, J. Elkins, G. Dutton, D. Fahey, H. Vömel, S. Oltmans, and K. Rosenlof (1999), Transport into the Northern Hemisphere lowermost stratosphere revealed by in situ tracer measurements, *J. Geophys. Res.*, *104*(D21), 26,565–26,580, doi:10.1029/1999JD900323.

Reid, S. J., A. F. Tuck, and G. Kiladis (2000), On the changing abundance of ozone minima at northern midlatitudes, *J. Geophys. Res.*, *105*(D10), 12,169–12,180.

Ridley, B. A., F. E. Grahek, and J. G. Walega (1992), A small, high-sensitivity, medium-response ozone detector for measurements from light aircraft, *J. Atmos. Oceanic Technol.*, *9*, 142–148.

Rind, D., P. Lonergan, and K. Shah (1996), Climatic effect of water vapor release in the upper troposphere, *J. Geophys. Res.*, *101*(D23), 29,395–29,405.

Rosenlof, K. H. (1995), Seasonal cycle of the residual mean meridional circulation in the stratosphere, *J. Geophys. Res.*, *100*, 5173–5191.

Rosenlof, K. H., A. F. Tuck, K. K. Kelly, J. M. Russell III, and M. P. McCormick (1997), Hemispheric asymmetries in the water vapor and inferences about transport in the lower stratosphere, *J. Geophys. Res.*, *102*(D11), 13,213–13,234.

Seo, K.-H., and K. P. Bowman (2001), A climatology of isentropic cross-tropopause exchange, *J. Geophys. Res.*, *106*(D22), 28,159–28,172, doi:10.1029/2000JD000295.

Seo, K.-H., and K. P. Bowman (2002), Lagrangian estimate of global stratosphere-troposphere mass exchange, *J. Geophys. Res.*, *107*(D21), 4555, doi:10.1029/2002JD002441.

Shapiro, M. A. (1980), Turbulent mixing within tropopause folds as a mechanism for the exchange of chemical constituents between stratosphere and troposphere, *J. Atmos. Sci.*, *37*, 994–1004.

Shepherd, T. G. (2007), Transport in the middle atmosphere, *J. Meteorol. Soc. of Jpn.*, *85B*, 165–191.

Solomon, S., K. H. Rosenlof, R. W. Portman, J. S. Daniel, S. M. Davis, T. J. Sanford, and G.-K. Plattner (2010), Contributions of stratospheric water vapor to decadal changes in the rate of global warming, *Science*, *327*, 1219–1223, doi:10.1126/science.1182488.

Sprenger, M., and H. Wernli (2003), A Northern Hemispheric climatology of cross-tropopause exchange for the ERA15 time period (1979–1993), *J. Geophys. Res.*, *108*(D12), 8521, doi:10.1029/2002JD002636.

Sprenger, M., C. M. Maspoli, and H. Wernli (2003), Tropopause folds and cross-tropopause exchange: A global investigation based upon ECMWF analyses for the time period March 2000 to February 2001, *J. Geophys. Res.*, *108*(D12), 8518, doi:10.1029/2002JD002587.

Stiller, G. P., et al. (2008), Global distribution of mean age of stratospheric air from MIPAS SF_6 measurements, *Atmos. Chem. Phys.*, *8*, 677–695.

Stohl, A. (1998), Computations, accuracy and applications of trajectories—A review and bibliography, *Atmos. Environ.*, *32*(6), 947–966.

Stohl, A., et al. (2003), Stratosphere-troposphere exchange: A review, and what we have learned from STACCATO, *J. Geophys. Res.*, *108*(D12), 8516, doi:10.1029/2002JD002490.

Stone, E. M., W. J. Randel, and J. l. Stanford (1999), Transport of passive tracers in baroclinic wave life cycles, *J. Atmos. Sci.*, *56*, 1364–1381.

Susskind, J., C. D. Barnet, and J. M. Blaisdell (2003), Retrieval of atmospheric and surface parameters from AIRS/AMSU/HSB data in the presence of clouds, *IEEE Trans. Geosci. Remote Sens.*, *41*, 390–409.

Tuck, A. F., S. J. Hovde, K. K. Kelly, M. J. Mahoney, M. H. Proffitt, E. C. Richard, and T. L. Thompson (2003), Exchange between the upper tropical troposphere and the lower stratosphere studied with aircraft observations, *J. Geophys. Res.*, *108*(D23), 4734, doi:10.1029/2003JD003399.

Vaughan, G., and C. Timmis (1998), Transport of near-tropopause air into the lower midlatitude stratosphere, *Q. J. R. Meteorol. Soc.*, *124*, 1559–1578.

Vaughan, G., D. Price, and A. Howells (1994), Transport into the troposphere in a tropopause fold, *Q. J. R. Meteorol. Soc.*, *120*, 1085–1103.

Waugh, D. W., and T. M. Hall (2002), Age of stratospheric air: Theory, observations, and models, *Rev. Geophys.*, *40*(4), 1010, doi:10.1029/2000RG000101.

Wernli, H., and M. Bourqui (2002), A Lagrangian "1-year climatology" of (deep) cross-tropopause exchange in the extratropical Northern Hemisphere, *J. Geophys. Res.*, *107*(D2), 4021, doi:10.1029/2001JD000812.

World Meteorological Organization (1957), Meteorology—A three-dimensional science. Second session of the commission for aerology, *WMO Bull.*, *4*(4), 134–138.

Zahn, A., and C. A. M. Brenninkmeijer (2002), New directions: A chemical tropopause defined, *Atmos. Environ.*, *37*(3), 439–440, doi:10.1016/S1352-2310(02)00901-9.

Zhong, W., and J. D. Haigh (1995), Improved broadband emissivity parameterization for water vapor cooling rate calculations, *J. Atmos. Sci.*, *52*, 124–138.

E. L. Atlas, Division of Marine and Atmospheric Chemistry, Rosenstiel School of Marine and Atmospheric Science, University of Miami, 4600 Rickenbacker Causeway, Miami, FL 33149, USA. (eatlas@rsmas.miami.edu)

K. P. Bowman, Department of Atmospheric Sciences, Texas A&M University, MS 3150, College Station, TX 77843, USA. (k-bowman@tamu.edu)

T. Campos, W. Hall, L. L. Pan, and A. Weinheimer, Atmospheric Chemistry Division, National Center for Atmospheric Research, PO Box 3000, Boulder, CO 80307-3000, USA. (campos@ucar.edu; hallb@ucar.edu; liwen@ucar.edu; wein@ucar.edu)

G. Günther, P. Konopka, R. Müller, and B. Vogel, Forschungszentrum Jülich, Institute of Energy and Climate Research - Stratosphere, D-52425 Jülich, Germany. (G.Guenther@fz-juelich.de; p.konopka@fz-juelich.de; ro.mueller@fz-juelich.de; b.vogel@fz-juelich.de)

I. Pollack, Chemical Sciences Division, Earth System Research Laboratory, NOAA, 325 Broadway, R/CSD, Boulder, CO 80305-3337, USA. (ilana.pollack@noaa.gov)

J. Wei, NASA Goddard Space Flight Center, Code 610.2, Greenbelt, MD 20771, USA. (jennifer.c.wei@nasa.gov)